Available online at www.sciencedirect.com
SCIENCE DIRECT®
International Journal of Rock Mechanics & Mining Sciences 43 (2006) 369–387
International Journal of Rock Mechanics and Mining Sciences
www.elsevier.com/locate/ijrmms

Influence of geotechnical factors on gas flow experienced in a UK longwall coal mine panel

D.N. Whittles[a,*], I.S. Lowndes[a], S.W. Kingman[a], C. Yates[b], S. Jobling[b]

[a]*Nottingham Mining and Minerals Centre, University of Nottingham, University Park, Nottingham, NG7 2RD, UK*
[b]*UK Coal Ltd., Harworth Park, Blyth Road, Doncaster, DN11 8DB, UK*

Accepted 27 July 2005
Available online 26 September 2005

Abstract

Methane drainage has become an integral part of modern coal mining operations when gas emissions cannot be practically dealt with using conventional ventilation methods alone. Boreholes are often drilled above and below the caving zone and connected to a drainage range located along the return gate. This paper describes the construction and analysis of the results obtained from the two- and three- dimensional geomechanical and gas flow models experienced around an active deep UK longwall coal production panel. The models constructed using the commercial FLAC codes were undertaken to provide information to the ventilation engineers at the mine on the likely gas sources and gas flow paths into the face line areas and gate roads. This information allows for the correct design of the orientation, length and support of the boreholes to maximise gas capture. The paper describes the method adopted to derive the relevant rock mass parameters and the laboratory tests conducted to obtain the stress-dependent permeability of coal measure rock strata. A functional relationship is proposed whereby the intrinsic bulk permeability of a sheared coal measure rock may be predicted from the confining stress. A detailed discussion of the geomechanical modelling methodology and the derivation of the strata permeabilities and gas flow modelling adopted is presented. The output of the models is described and used to interpret the major potential gas sources and pathway into the workings.

Keywords: Longwall mining; Geomechanical modeling; Methane drainage; Stress-dependant permeability

1. Introduction

As the production rates obtained from modern high-performance retreat longwall faces increase, there is a need to maintain and improve the capture performance of methane drainage ranges. The methane drainage boreholes which are often drilled above and below the caving zone are connected to a drainage range located along the return gate. To maintain the capture efficiency of the boreholes and ranges requires an understanding of both the caving mechanics and the movement of gas within the waste and the return gate road.

The stress and fracture zones created by the extraction and caving process in the vicinity of high-production retreat longwall faces strongly influence the emission of gas into these mine workings. The stress distribution has a major influence on the bulk volume permeability of the fractured and disturbed zone. The changes in permeability upon longwall extraction promote the release and enhanced flow of strata gases from seams above and below the extraction horizon into the waste and mine workings.

The stress distribution formed across the waste may be classified into three distinct stress distribution zones. As a longwall face retreats, the loading of the overbearing strata on the face supports is projected forward 10–20 m ahead of the face, creating what is known as the stress abutment zone. The stress abutment promotes

*Corresponding author. Tel.: +44 115 9514104; fax: +44 115 9513898.
E-mail address: david.whittles@nottingham.ac.uk (D.N. Whittles).

1365-1609/$ - see front matter © 2005 Elsevier Ltd. All rights reserved.
doi:10.1016/j.ijrmms.2005.07.006

vertical fracture planes extending above and below the working horizon. These fracture zones often intersect gas bearing Coal Measures at pressures that release the adsorbed and absorbed gas content to the relatively low-pressure waste and mine workings [1]. The effect of the mining may therefore cause gas to migrate from adjacent coal seams into the active mine workings under a gas pressure gradient [2]. It has recently been estimated [1] that as much as 90 percent of the methane entering a longwall district may come from adjacent seams. As a consequence of longwall coal mining, the gas permeabilities of the rock strata are substantially increased by the development and dilation of joints, bedding planes and mining-induced fractures. The opening of fractures due to the mining disturbance is also responsible for the release of methane gas adsorbed within adjacent coal seams by increasing the exposed surface area of the coal.

The zone of newly caved waste immediately behind the supports forms a region of relatively low stress. This low loading allows for a penetration of the ventilation air from the face travel-way into the caved waste. This ventilation air flow leakage keeps the fringe of any strata gases present back into the waste and flushes the waste gases to the return gate of the face. At distances further behind the face line, the stress load increases as the caved waste undergoes a re-compaction and recovers to a stress distribution just below that of the virgin field.

To understand the nature of gas flow around a longwall panel, there is a need to characterise the potential role of predominant fracture flow paths to the emission of gases through a fractured/permeable region. It has long been recognised that improved numerical modelling techniques are required to more accurately simulate the large-scale deformation around underground excavations, which define the potential flow paths of strata gases. However, to effectively model the deformation requires a determination of rock mass properties of the surrounding strata. Recent research work carried out at the University of Nottingham has resulted in the development of an accurate rock mass classification method for UK Coal Measures [3]. This rock mass classification can be used to generate a range of strength and stiffness parameters necessary to create a representative geomechanical numerical model [4]. Given a defined extraction sequence and geometry, geomechanical modelling may be employed to predict the deformations, failure zones and stresses around the excavations [5].

The stress–permeability behaviour of coal or Coal Measure strata is the key to the effective simulation of methane flow. It is essential that the bulk stress–permeability relationship (pre- and post-failure) be well understood before a reliable predictive model can be constructed for a longwall coalface. Fundamental studies have been carried out at the University of Nottingham to investigate the stress–permeability relationship [6–8] and the modelling of methane flow around a longwall face [9–12]. A more recent study established the post-failure stress–permeability behaviour of Coal Measure rocks and applied computational fluid dynamics (CFD) to model the resultant flow of methane into mine workings [13–17].

This paper details the results of a program of geomechanical modelling conducted on the 43s retreat longwall coal panel at Thoresby Colliery, UK Coal Ltd., North Nottinghamshire, UK. In order to maintain safe working levels of gas within the longwall panel methane drainage was undertaken. The drainage range consisted of 75 mm ID diameter boreholes drilled at regular spacings into the roof and floor of the tailgate roadway inclined at an angle of 60° over the goaf. The panel was situated at a depth of approximately 770 m and was 270 m wide.

To provide information to the environmental engineers responsible for the gas drainage, both two-dimensional and three-dimensional numerical modelling using the FLAC [2,18] software code was undertaken. The modelling provided information on the presence of rock fractures that act as gas pathways, the horizons within the roof which were potential gas sources and on the changing stress condition around the face that affects the strata permeabilities.

1.1. Thoresby Colliery

Thoresby Colliery is located in the north of the county of Nottinghamshire, 32 km northeast of the city of Nottingham Fig. 1. The colliery was established between 1925 and 1928, and since this time production has been concentrated within High Hazels, Top Hard and Parkgate coal seams.

The privatisation of the UK coalfields occurred in 1993 when RJB Mining (now UK Coal plc) assumed ownership of the mine. The current mineral production of the mine is restricted to the Parkgate seam that is 770 m beneath the surface. Coal is currently being extracted from the number 43 longwall panel.

1.2. Production and layout detail of the 43s longwall face

Panel 43 consisted of a retreat longwall panel with a 270 m wide face. Coal extraction was by a ranging arm shearer with the roof of the face line supported by hydraulically powered supports Fig. 2. The height of extraction was 2 m, and the proposed length of the panel was 2000 m. Ventilation and access to the face line of the panel was provided by two pre-driven gate roads running either side along the length of the panel. The access gate roads were 4.9 m wide and 3 m high. The primary support system used within the gate road

Fig. 1. Location of Thoresby Colliery, Nottinghamshire, UK.

consisted of rows of 6, 2.4 m long full column grouted roof bolts.

1.3. Methane drainage of panel 43

Methane drainage was practised across panel 43 to maintain safe working conditions within the gate roads and face line of the longwall panel. The exact source beds of the methane ingress were unknown, but from a combination of previous experience and an analysis of the geological data obtained from exploration boreholes, it was determined that the most likely sources were considered to be the Parkgate seam itself and underlying and overlying coal seams and carbonaceous beds in the immediate vicinity above and below the extracted coal seam. The methane drainage boreholes consisted of 75 mm diameter holes bored into the roof and floor of the tailgate immediately behind the face line. Standpipes were partially installed within the boreholes as the highly fractured strata present within the immediate roof precluded satisfactorily sealing the borehole. The roof boreholes were inclined over the goaf at an angle of approximately 60° above the horizontal whilst the floor boreholes were inclined under the base of the goaf at an angle of 60° below the horizontal. The roof holes were 60 m long and the floor boreholes were 20 m long. The length and orientation of the drainage boreholes was selected on the basis of the results achieved on previously worked adjacent panels.

2. Geological and rock strata characterisation

To construct a numerical geotechnical model of the longwall panel, a detailed knowledge of the geological properties of the surrounding rock strata, the measured in-situ stress conditions and the longwall geometry was required. The colliery geologist and geotechnical engineer supplied a range of technical data, which included detail of relevant geological borehole logs, the unconfined compressive strength and Young's modulus of the rock strata obtained from cored boreholes, the layout of the longwall panels and the orientation and length of the methane drainage boreholes.

2.1. Determined rock properties

Laboratory test values for the unconfined compressive strength and Young's modulus of rock samples were obtained from cored boreholes drilled at four locations in the roof of the main gate of the adjacent 42s panel. A summary of the results determined from these tests is presented in Table 1. An analysis of the experimental data concluded that the immediate roof of the Parkgate seam in the vicinity of panel 43 had average values of 13.47 GPa and 60.8 MPa for the Young's modulus and unconfined compressive strength (UCS), respectively.

In general, to account for structural features which are present in the rock mass, laboratory test results obtained from rock strata samples need to be recast to represent in-situ values. This translation is often undertaken using a rock mass classification value usually obtained from either the Rock Mass Rating [20] or the [21] Quality Factor classification systems. However, such general classification systems are not specific to the characteristics exhibited by UK Coal Measure rock strata. Previous research undertaken at the University of Nottingham concluded that the in-situ strengths and stiffnesses of coal measure lithologies are dependent on various parameters such as bedding, jointing and fissility. In addition, it was concluded that the mechanical properties of Coal Measure rock strata are usually anisotropic, exhibiting different properties in a direction parallel to the bedding. This research has led to the development of a modified Rock Mass Rating system, with weightings and parameters evaluated specifically for UK Coal Measure strata [3].

The geological borehole information obtained from the colliery engineering staff was used to construct a simplified geological model of the strata surrounding the 43s longwall panel. The borehole logs were resolved into basic lithological units (listed in Appendix A), whilst the mine plans indicated that the rock strata was approximately horizontal. Although the geological test data, as detailed in Table 1, was available for strata surrounding the adjacent panel number 41, no structural descriptions

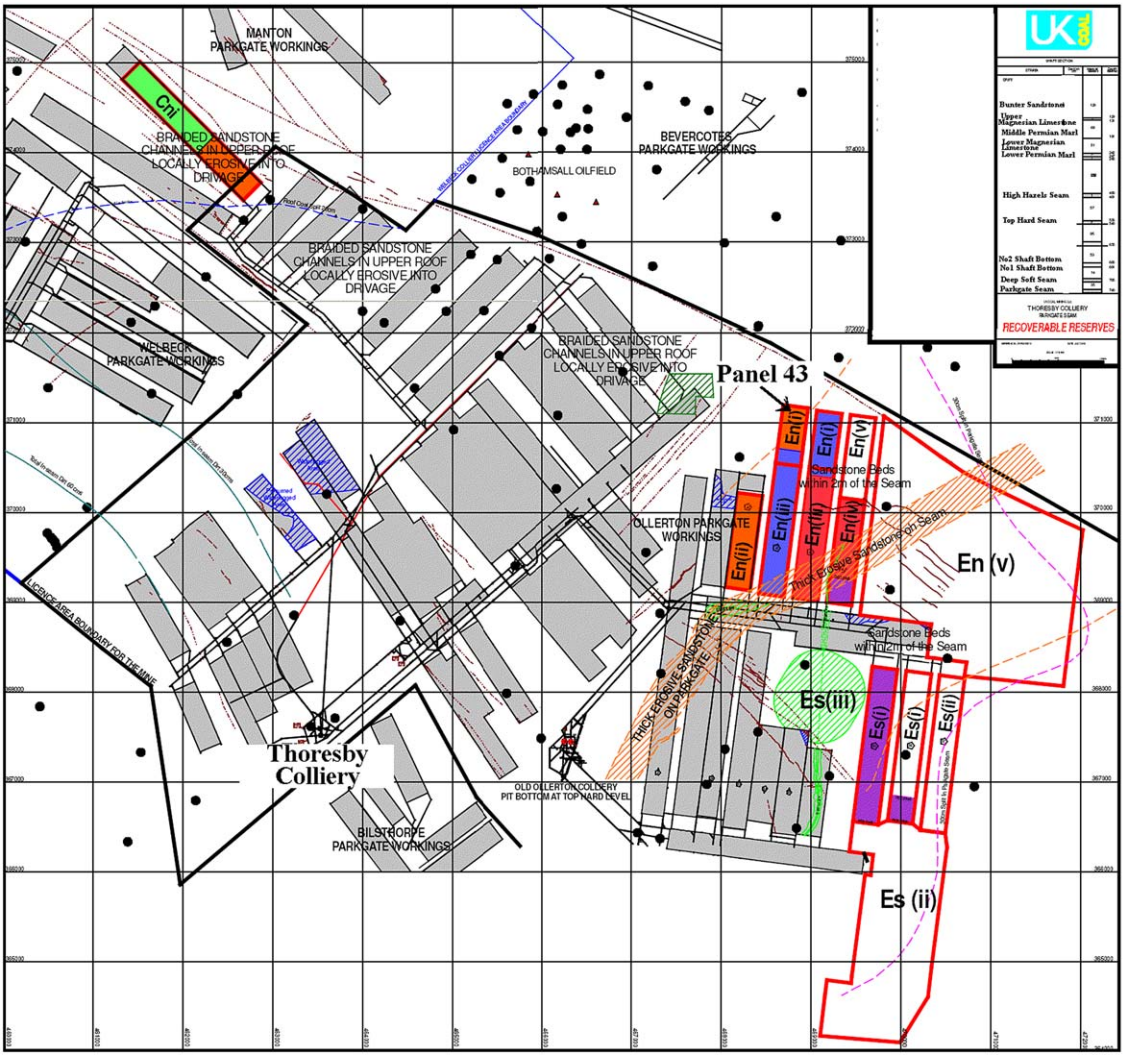

Fig. 2. Layout of projected longwall panels in the Parkgate seam, Thoresby Colliery (adapted from DTI [19]).

Table 1
Laboratory test values for the rock core samples taken from the immediate roof of panel 41, adjacent to panel 42

Borehole ref metre mark	Height above seam (m)	Lithology	Sample length (mm)	Average diameter (mm)	UCS (MPa)	Young's modulus (GPa)
312	0.9	Sandstone	84.33	43.97	75.8	13.95
312	2.5	Laminated siltstone	84.02	44.65	45.5	10.40
312	5.4	Sandstone	83.96	44.07	63.4	15.72
510	1.85	Laminated sandstone	83.95	43.24	60.8	13.02
510	3.10	Sandstone	84.01	43.73	67.9	17.97
510	4.80	Sandstone	84.02	42.57	72.4	15.28
716	1.30	Sandstone	84.07	44.36	61.0	12.68
716	2.40	Laminated sandstone	80.95	43.90	47.1	10.70
716	3.8	Laminated siltstone	84.12	44.16	64.3	14.77
843	1.50	Laminated siltstone /sandstone	84.13	44.75	56.3	11.45
843	2.80	Laminated siltstone	84.10	44.52	51.6	11.15
843	4.08	Sandstone	83.62	43.89	63.8	14.50

were available for either panel 42 or 43. This is typical of most rock engineering problems, where due to the difficulty in obtaining and testing samples, only limited data, usually in the form of basic lithological descriptions obtained from open hole borehole logs, is available. The mechanical properties required for

the modelling such as the intact rock Young's modulus, unconfined compressive strength and rock mass classification ratings were derived from laboratory tests synthesised with data obtained from a database of properties and rock mass ratings for similar strata types held by the University of Nottingham. Typical classification ratings of coal measure rock strata identified by classification of roof cores taken from the gate roads of a number of UK coal mines are shown in Table 2.

The in-situ strength and stiffness parameters required for the constitutive models of the rock strata used in the FLAC modelling were determined using an in-house Visual Basic software application. The programme utilised a Hoek-Brown rock mass failure criterion [22] to determine the average friction and cohesion strength parameters over the range of confining stresses that were estimated to develop around the longwall panel. The input data required to determine the strength parameters using this criterion included the unconfined compressive strengths of the strata, the rock mass ratings and the rock types (Table 3).

To estimate the in-situ modulus of deformation of the different lithological units, an empirically derived relationship between rock mass rating value and intact Young's modulus was used [23]:

$$E_{\text{def}} = 0.5E\left[1 - \left(\cos\left(\pi\frac{RMR}{100}\right)\right)\right], \quad (1)$$

Table 2
Rock mass ratings for UK coal measure strata [1]

Lithology	Bedding rating	Matrix rating	Anisotropic ratio
Fissile mudstone	31→38	46→50	1.32→1.44
Silty mudstone	40→46	52→57	1.22→1.30
Laminated siltstone	38→44	52→58	1.28→1.39
Massive siltstone	48→64	58→66	1.00→1.21
Laminated sandstone	46→62	58→64	1.10→1.26
Coal	58→62	49→60	0.89→0.91

where E_{def} is the deformation modulus (GPa), E the intact Young's modulus (GPa) and RMR the rock mass rating (0–100).

3. Height of the cave and goaf characteristics

The height of the cave of the roof stratum above the extracted coal seam and the compaction characteristics of the broken rock within the goaf have a significant influence on the strains, fracture patterns and redistributed stress field that occur within the rock strata as a result of longwall mining. To satisfactorily model the geological effects produced by longwall mining, it is important to represent correctly the thickness and compaction properties of the goaf. Several researchers have proposed relationships between the imposed stress and the degree of volumetric compaction [24,25]. However, the most recent formulae to estimate caving height and goaf compaction have been proposed by Yavuz [26]. These relationships were adapted from an analysis of previous theoretical studies and observations. Yavuz formulae were used in this study to model the stress–strain behaviour of the goaf of Thoresby Collieries 43s longwall panel. To estimate the height of the cave of the roof stratum above the Parkgate seam, the expression contained within Eq. (2) was employed [26]:

$$H_c = \frac{100h}{c_1 h + c_2}, \quad (2)$$

where H_c is the caving height (m), h is the height of extraction (m) and C_1 and C_2 (coefficients) have been empirically derived depending on stratum lithology (Table 4).

The laboratory test data obtained from the immediate roof stratum of the adjacent longwall coal panel 42 (Table 1) indicated a medium strong roof to the Parkgate seam in the vicinity of the panel with an average roof unconfined compressive strength of

Table 3
Determined mechanical properties of the rock strata surrounding the 43s longwall panel, Thoresby Colliery

Rock type	UCS (MPa)	Young's modulus	Average CMC	Horizontal CMC	Vertical CMC	Stiffness (GPa)	Bedding strength			Joint strength		
							ϕ	c	t	ϕ	c	t
Siltstone and sandstone	70	20	58	54.0	61.0	12.49	46	1.53	−0.1	47	1.95	−0.3
Coal seatearth	40	4	42	35.0	48.0	1.56	29	0.15	0	32	0.71	0
Silstone	70	20	59	56.0	62.0	12.79	44	1.21	−0.1	45	1.45	−0.2
Mudstone seatearth	40	8	42	35.0	48.0	3.005	33	0.66	0	37	0.84	0
Mudstone/coal/ seatearth	40	8	42	35.0	48.0	3.005	33	0.66	0	37	0.84	0
Seatearth	20	8	42	35.0	48.0	3.004	28	0.5	0	32	0.61	0
Mudstone	60	15	48	43.0	54.0	7.029	48	1.32	−0.1	50	1.79	−0.2
Sandstone	120	25	58	54.0	61.0	15.61	50	2.14	0	51	2.85	−0.3
Coal	30	8	57	60.0	54.0	4.87	33	0.83	0	32	0.71	0

Table 4
Values of the coefficients C_1 and C_2 for various strengths of strata

	C_1	C_2
Strong and hard	2.1	16
Medium strong	4.7	19
Soft and weak	6.2	32

Table 5
Determined goaf compaction parameters

Parameter	Roof condition		
	Strong and hard	Medium strong	Soft and weak
σ_c (MPa)	100	60	10
B	1.202	1.284	1.444
Eo (MPa)	306	108	7
ε_m	0.17	0.22	0.31

60 MPa. Assuming an average mineral extraction height of 2 m (corresponding to the average thickness of the Parkgate seam), an estimated caving height of 7 m above the seam was calculated from Eq. (2).

3.1. Determination of the degree of goaf compaction

Employing the method proposed by Yavuz [26], Eq. (3) below was used to define the relationship between stress conditions and the degree of plastic strain experienced within the goaf:

$$\sigma = \frac{Eo\varepsilon}{1-\varepsilon/\varepsilon_m}, \tag{3}$$

where, σ is the average stress in the goaf $(\sigma_1+\sigma_2+\sigma_1)/3$ (Pa), b the bulking factor of the broken strata, ε the volumetric plastic strain, σ_c the unconfined compressive strength of the intact rock, (Pa), Eo the initial tangential modulus (Pa) and ε_m the maximum possible strain of the bulked rock material.

The following relationships were used to calculate the values for the parameters Eo, b and ε_m [26]:

$$Eo = \frac{10.39\sigma_c^{1.042}}{b^{7.7}}, \tag{4}$$

$$b = \left(\frac{c_1 h + c_2}{100}\right) + 1, \tag{5}$$

$$\varepsilon_m = \frac{b-1}{b}. \tag{6}$$

The parameters relating to goaf compaction determined for an extraction height of 2 m for the three conditions is given in Table 5.

To construct the geotechnical model it was assumed that the roof stratum was assumed to be medium strong (as indicated by the laboratory test data) and the corresponding stress–strain relationships for the goaf were determined using Eqs. (3)–(6).

4. Results of the laboratory test conducted to determine stress-dependent permeability of the strata

Research into the permeability characteristics of UK Coal Measure rock strata has concluded that as coal measure rock fails and fracture occurs, the permeability rises rapidly. These results suggest that fracture permeability may be a dominant factor in determining the gas flow paths into working areas from adjacent coal seams or gas bearing horizons [27,28].

For this study, to develop a relationship between stress and stratum permeability, a series of laboratory experiments using a test method devised by Durucan [8] were undertaken on both intact and fractured coal measure siltstone samples. The experiments were undertaken on five samples of a fine-grained coal measure siltstone that can be considered typical of the major proportion of the coal measure sequence around the 43s longwall panel [29]. The siltstone test samples were prepared into cylindrical cores 37.5 mm in diameter and 75 mm long. In turn the prepared core samples were placed into a Hoek-Cell which also acted as a permeameter. The sample was supported in a stiff press between steel perforated end platens. Nitrogen gas was injected into the top of the sample at a pressure of 0.276 MPa. The volumetric flow rate of gas through the sample was monitored during the test using gas flow meters connected via a plastic tube to the bottom platen. To determine the intact permeability of the siltstone, an initial confining stress of 0.5 MPa was applied to the sample and then the sample was axially loaded such that the axial stress was equal to 3 times the confining stress until a final confining stress of 8 MPa was obtained. As each increment of stress ratio was increased, the loading on the stiff press was put on hold to allow a flow reading to be taken.

To investigate the permeability of fractured siltstone, the final increment of confining stress on the intact sample was reduced to 0.5 MPa and the axial stress increased until failure of the sample occurred. The process of reapplication of the stress ratio starting from 0.5 to 8 MPa confining stress at 0.5 MPa increments whilst increasing the axial stress in a ratio of 3 times the confining stress was undertaken with flow readings being taken at each increment in confining stress.

The intrinsic permeability at each confining pressure was then calculated using.

$$k_i = \frac{Q\mu L}{A\Delta p}, \tag{7}$$

where k_i is the intrinsic permeability (m^2), Q the volumetric flow rate (m^3/s), μ the viscosity (Ns/m^2), A

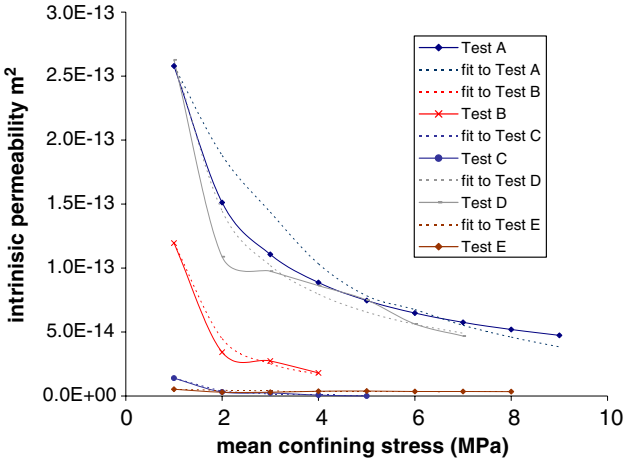

Fig. 3. Graphical representation of the experimental results of laboratory tests conducted to determine the stress-dependent permeability of siltstone rock samples.

the cross-sectional area (m^2), Δp the pressure drop over length of sample (N/m^2) and L the length of sample (m).

It was found in all cases that the permeability of the intact siltstones was lower than the detection limit of the flow meters, giving an intact permeability of less than $1 \times 10^{-19}\,m^2$.

A graphical representation of the data obtained from the tests performed on the five fractured siltstone samples is shown as the solid lines in Fig. 3. From an analysis of the data represented in the figure, it may be concluded that the gas permeability of the sheared samples decreases rapidly as the confining pressure increases over the range 0.5–4 MPa.

A further analysis of the data was undertaken to develop a functional material parameter that can be coded into the numerical models to predict the distribution of permeability of the fracture planes that develop around the panel. The functional relationship that was found to provide the best fit to the test data is represented as

$$K(\sigma_1, \sigma_2) = K_1 \left(\frac{\sigma_1 + \sigma_3}{2}\right)^m, \tag{8}$$

where K is the intrinsic permeability (m^2), σ_1 and σ_3 are the minimum and maximum confining stresses (MPa), K_1 is the intrinsic permeability (m^2) when $(\sigma_1 + \sigma_3)/2 = 1$ MPa and m is a material parameter found by regression analysis.

The test data and the predicted permeabilities for the five tests are shown in Fig. 3.

5. Geotechnical modelling of the longwall panel

Two-dimensional and three-dimensional geomechanical models of panel 43 were constructed using the FLAC software codes. The three-dimensional modelling was undertaken first, to validate the material models of the rock strata and goaf to compare the modelled stress redistributions to those predicted by established empirical methods. The three-dimensional model was also used to determine the degree of goaf compaction predicted behind the face line. This information was subsequently used to identify the relevant positions of the two-dimensional model sections.

5.1. FLAC^{3D} three-dimensional geotechnical modelling

An initial three-dimensional computational model was constructed to represent the longwall panel using the geotechnical software code FLAC^{3D} [18]. This model was developed to study the variation of the volumetric compaction across the goaf area and to identify the three-dimensional stress redistribution around the panel.

The representative model geometry constructed was 1200 m long, 1070 m high and 600 m wide. The model was subdivided into a mesh of sub-blocks of varying size dependent on the variation of the expected stress field. Within areas of high stress, such as within the vicinity of the longwall face line and stress abutment zone, smaller blocks of dimension $2\,m \times 5\,m \times 5\,m$ were employed. However, in the periphery areas of the model away from the panel, larger $10\,m \times 5\,m \times 5\,m$ blocks were employed. The final model was formed from 560,000 sub-blocks. The dimensions of the geometry of the geotechnical model are shown in Fig. 4.

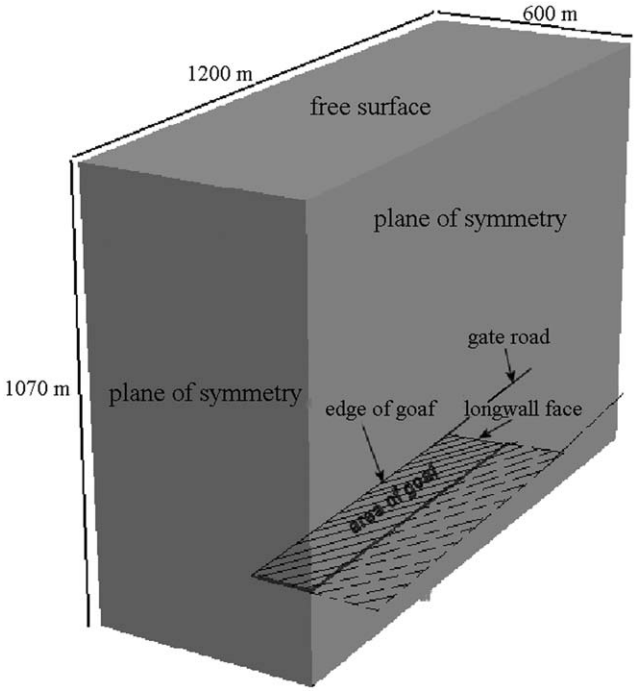

Fig. 4. Geometry of the initial geotechnical model showing the position of boundaries representing planes of reflective symmetry.

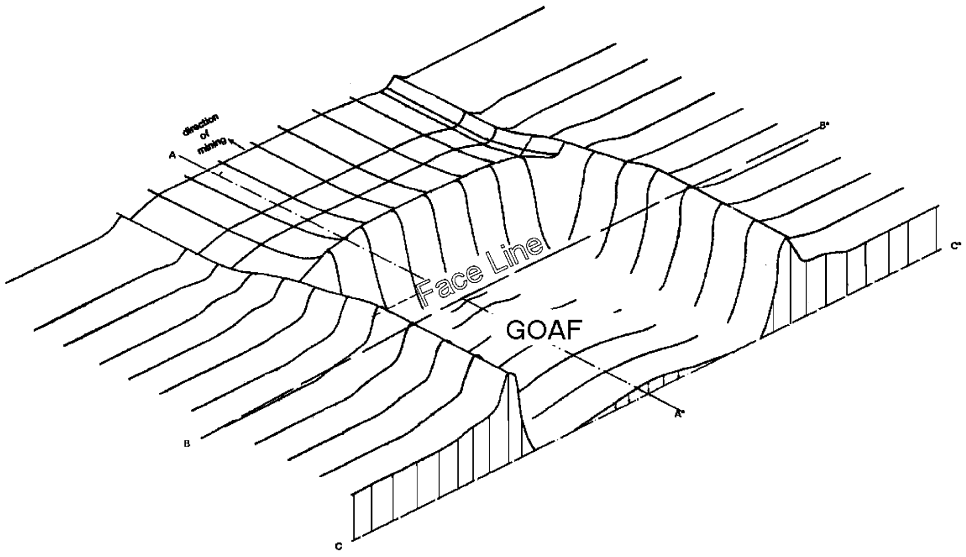

Fig. 5. Vertical stress distribution (vertical axis) around a retreat longwall panel (after Peng and Chiang [32]).

5.1.1. Boundary and initial conditions

5.1.1.1. Boundary conditions. The natural symmetry of panel 43 was exploited in the modelling performed to reduce both the model size and the computational time. The side boundaries of the FLAC^{3D} model were prevented from moving in the horizontal direction. The effect of this condition was such that these boundaries acted as planes of reflective symmetry (Fig. 5).

5.1.1.2. Initial stress conditions. Vertical stress. Within the interior of the model the vertical stresses were assumed to increase linearly with depth due to the weight of the overlying rock strata. The density of the rock strata was assumed to be 2500 kg/m^3. The initial vertical stress varied from 26.75 MPa at the base of the model to 0 MPa at the surface, whilst at the depth of the panel the vertical stress was predicted to be 19.25 MPa.

Horizontal Stress. Within the UK coalfields the horizontal stresses are affected by tectonic strain and therefore cannot be directly determined from the lateral restraint provided by the vertical loading [30,31]. Stress measurements taken within the Parkgate seam at Thoresby Colliery indicated a maximum horizontal stress of 17 MPa [30]. This horizontal stress measurement was a factor 0.88 lower than the predicted vertical stress. Thus in the solution of the geotechnical model the initial values of the horizontal stresses were set equal to the measured maximum vertical stress multiplied by this factor.

5.1.2. Validation of the FLAC^{3D} geotechnical model

The extraction of coal in a longwall panel leads to the redistribution of the in-situ vertical stress into the strata on the periphery of the panel. Enhanced zones of stress relative to the in-situ stress are created close to the periphery of the extracted area and reduced stress zones are created within the worked-out area (Fig. 5) [32]. Immediately adjacent to the panel, the increase in vertical load leads to rock failure and yield zone development.

A series of validation exercises of the model were undertaken to compare the modelled vertical stress redistribution around panel 43 to that predicted by established empirical formulae. In the absence of the actual stress and displacement measurements taken in the rock strata around panel 43, the predicted numerical stress distributions were compared to those determined from an established empirical model developed to estimate the vertical stress pattern around the panel proposed by Wilson [33].

A solution to the initial geotechnical model was obtained by iterative numerical calculation to provide a condition of static equilibrium. This solution was resolved after approximately 48 h, employing 10,000 iterative time steps on a Pentium P4, 3.2 GHz computer processor.

For the comparative exercises performed, the following common data set was employed: a mining depth of 770 m, a longwall panel width of 270 m and an extraction height of 2 m, a rock mass UCS of 4.6 MPa and a triaxial stress factor of 3 was adopted.

From an analysis of the data presented in Fig. 6 it can be observed that the numerical model predicted a yield zone of approximately 10 m and a peak abutment stress of 62 MPa.These values were in close agreement to those determined from the Wilson model, which predicted a yield zone of 12 m and a coincident peak abutment stress of 62 MPa. Although the rate of the decay of the stress abutment predicted by the FLAC model was more rapid than that predicted by the empirical model, it was

concluded that in general the numerical model satisfactorily predicted the correct behaviour.

5.1.3. Roof displacement vs. distance behind the coalface

To investigate the behaviour of the caving experienced behind the longwall face following extraction, the downward displacements of the roof stratum predicted by the FLAC^{3D} model along a line drawn along the central axis of the panel were examined. It was concluded that the maximum predicted vertical roof displacement was 1.12 m. The displacement of the roof stratum at a level corresponding to the top of the goaf in front of the face, across the face line and then along the central symmetry axis of the goaf is plotted in Fig. 7 as a percentage of the maximum vertical roof displacement.

An analysis of the data presented in Fig. 7 concludes that the rate of roof movement was greatest in the initial 100 m behind the face line and that 90% of the roof movement had occurred by approximately 120 m behind the face.

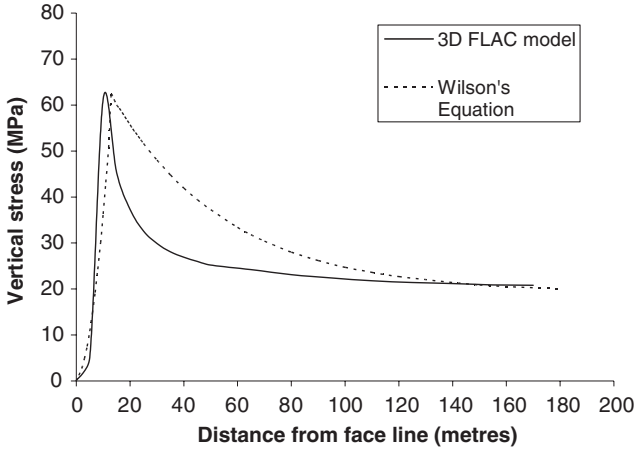

Fig. 6. Front abutment stress predicted by the modelling and predicted using Wilson's empirical method.

5.2. FLAC^{2D} two-dimensional geotechnical modelling

As an extension to the three-dimensional numerical models, a series of two-dimensional numerical models were constructed to investigate the plane strain problems associated with longwall extraction systems. The two-dimensional models represent vertical sections, parallel to the face line, passing through the goaf and gate roads. As with the solution of any numerical technique the accuracy of the results obtained depends on the detail and refinement of the grid used to represent the physical system. In general, a finer grid leads to more accurate results. This is especially true for the prediction of fracture or shear planes within the rock strata. The shear planes develop within numerical FLAC models by a process of strain localisation. In particular, previous studies [4] have found that finer grid resolutions were able to predict more realistic patterns of shear bands. Consequently, a fine grid resolution was chosen in a region around the face line to capture a realistic fracture pattern.

A section through the model section that shows the detail of the geology and two-dimensional structure of the strata around the panel within the model is illustrated in Fig. 8. The complete model dimensions extended for a horizontal distance of 1080 m and a vertical height of 900 m and consisted of 280,000 zones.

5.2.1. The modelling methodology adopted

The modelling methodology adopted in the FLAC^{2D} modelling is illustrated by the flow chart in Fig. 9. The dark grey shaded boxes in the figure represent the

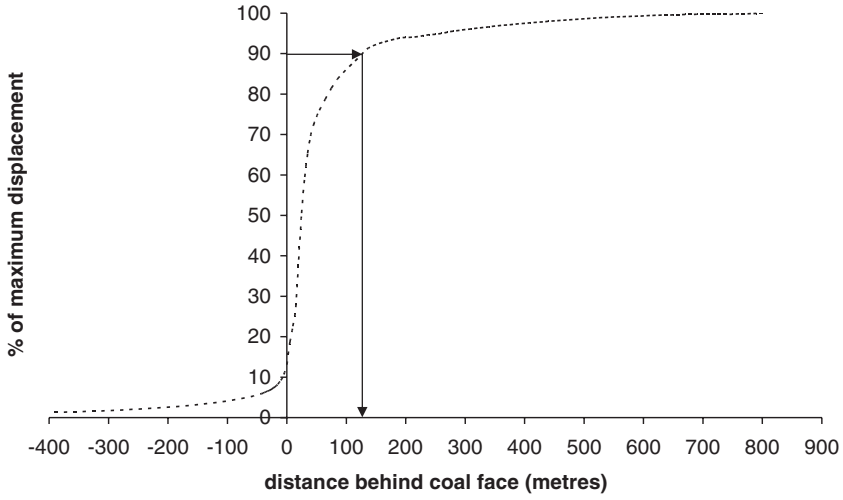

Fig. 7. Percentage of predicted maximum roof displacement experienced across the symmetry line drawn across the intact coal seam, the longwall face line and goaf.

acquisition of the model input data. The pale grey shaded boxes represent the modelling processes whilst the unshaded boxes represent the iterative model optimisation procedures and model solution output.

The redistribution of the in-situ stress field, the extent of broken ground and the development of major fractures around a longwall panel occur progressively with the extraction of the coal [32]. The permeability of a rock field to gas flow is strongly dependent on the state of compression of the rock strata. Consequently, the strata permeability and gas flow regime varies behind the face line as the goaf compacts under the force of the bridging beds lowering on the goaf. Thus, the ability to obtain effective gas capture from drainage boreholes located above and below the goaf changes progressively along the gate road with increasing distance behind the face line.

To investigate these changes, numerical models were constructed to represent the three stages of goaf compaction represented by the following regions:

- Model 1: uncompacted goaf.
- Model 2: partially compacted goaf.
- Model 3: fully compacted goaf.

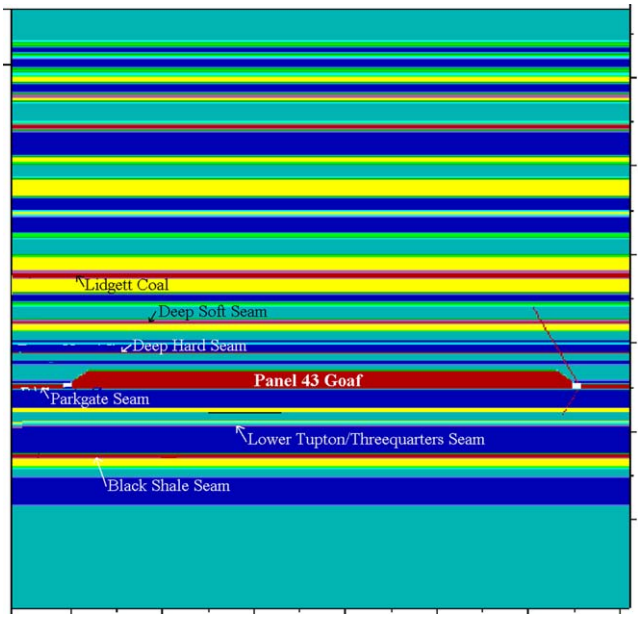

Fig. 8. Part of the FLAC^{2D} model showing the location of the 43s longwall panel, goaf and strata horizons.

5.2.2. Analysis of the solutions to the 2D FLAC^{2D} geotechnical models

5.2.2.1. Model 1: immediately behind the face line. After an initialisation of the in-situ stress field, the coal and immediate roof of the panel were removed and replaced by a goaf extending to a height of 7 m above the top of the coal seam. This was to simulate the removal of the coal seam due to longwall extraction. Time stepping mechanical computations were undertaken until a small amount of vertical displacement of the bridging beds downwards onto the goaf had occurred. The vertical displacement of the bridging beds was monitored during the modelling by a history log of the vertical displacement of the stratum directly overlying the goaf in the centre of the panel. This monitored vertical displacement represented 16% of the maximum vertical displacement which was determined from the final stage model, Model 3. From Fig. 7 this percentage of convergence represented a distance of approximately 10 m behind the face line.

The regions around panel 43 where the stress confinement was predicted to be less than 3 MPa are

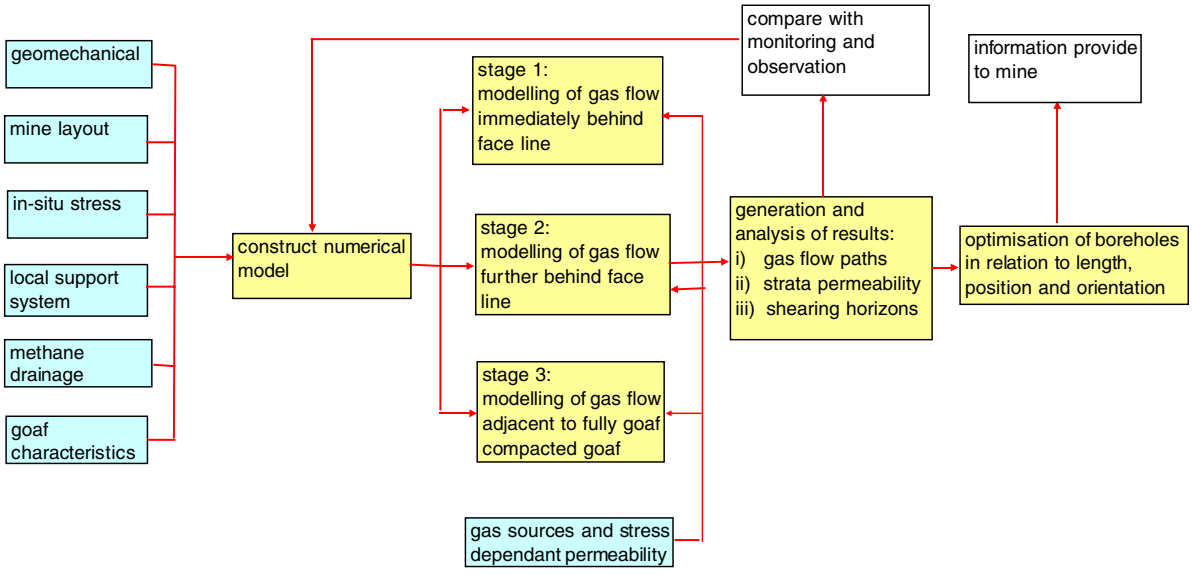

Fig. 9. Modelling methodology.

shown in Fig. 10. This limit value was chosen, since the laboratory test work on the fractured coal measure rocks indicated that the permeability was substantially reduced in areas where the confining stress was greater than 3 MPa [34,35].

The model predicted that fully developed shear planes would be limited to the edges of the goaf and to small localised zones around the roadways (Fig. 10). Due to the dilation of the planes that would occur during such shearing, these planes provide potential pathways for gas flow from surrounding gas bearing strata into the mine roadways. From an analysis of the laboratory shear box test data obtained by Denby [35], a shear strain increment of greater than 10 mm per metre was chosen to represent a fully developed shear plane.

5.2.2.2. Model 2: partially compacted goaf. Model 1 was then restored and the time stepping computations were continued until the monitored vertical roof displacement represented 80% of the vertical roof displacement. A comparison of this predicted displacement percentage with the data presented in Fig. 7 indicated a distance of approximately 65 m behind the face line.

The predicted regions around panel 43 where stress confinement is less than 3 MPa are shown in Fig. 11. Comparing this figure to Fig. 10 it can be seen that the regions of low confining stress, and therefore enhanced strata permeabilities, have increased significantly, extending in a broad region from within the goaf into the overlying roof beds to a height of approximately 180 m.

Fig. 11 also predicted that steeply dipping shear planes would originate from the roadways and extend over the goaf to a height of approximately 30 m. Horizontal shear planes are also predicted to occur at several distinct horizons in the regions around the edges of the panels. Several of these horizons are shown to be present at a height greater than 100 m. However, it was concluded that these shear horizons would be isolated from any potential continuous flow pathway for gas into the active mine workings.

5.2.2.3. Model 3: fully compacted goaf. The computational models were solved until a state of static equilibrium was obtained. The monitored vertical roof displacement of the bridging beds was 1.29 m, representing 100% of vertical displacement of the bridging beds and full goaf compaction. In the FLAC^{3D} model 90% goaf compaction occurred at a distance behind the face line of greater than 120 m (Fig. 7) and so Model 3 can be considered to represent a distance behind the face line of greater than 120 m.

The regions around panel 43 where stress confinement was predicted to be less than 3 MPa are shown in Fig. 12. On comparison of the data presented in Figs. 11 and 12 it can be seen that the region directly above the goaf present in Model 2, where the stress was lower than 3 MPa, is no longer present. This is due to stress build-up

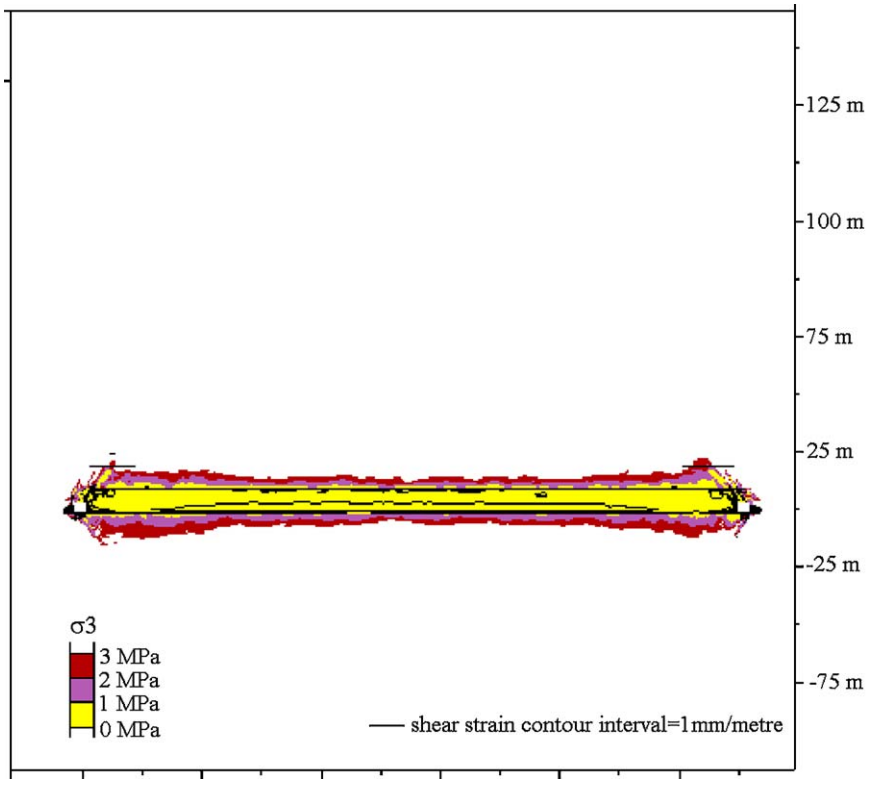

Fig. 10. Model 1: confining stress and shear strain developed around panel 43.

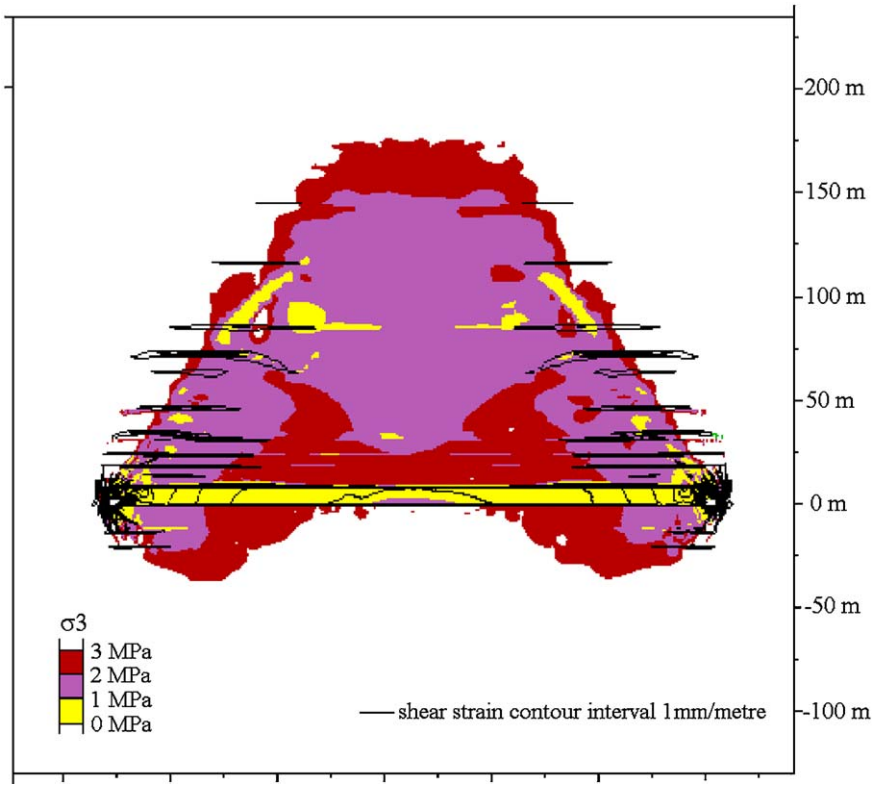

Fig. 11. Model 2: confining stress and shear planes around panel 43.

in the roof stratum as the goaf resists the downward movement of the bridging beds. The modelling also indicated that no further development of fracture planes compared to that for Model 2 had occurred.

6. Numerical modelling of gas flow around the panels

To produce an effective gas drainage system for panel 43, the drainage boreholes drilled into the roof and floor of the tailgate have to intercept the main gas flow pathways from the coal seams and strata that act as potential gas sources. To predict the position of these pathways and sources, flow modelling was undertaken using an adaptation of the fluid flow facility present in the FLAC code. The FLAC^{2D} geomechanical modelling indicated that the conditions most conducive to gas flow were present in Model 2, representing an approximate distance behind the face line of 65 m. This model was therefore used for the gas flow modelling. The fluid flow computational modelling available within the FLAC software code assumes Darcian flow through a semiporous medium with the rate of flow directly proportional to the strata permeability and the fluid pressure gradient.

6.1. Strata permeability

Zones of different strata permeabilities develop around a longwall panel as a result of the fracturing of the rock strata and the redistribution of the in-situ stress field (Fig. 13).

From an analysis of the results of the geomechanical modelling described in Section 5, it was concluded that there were four characteristic regions of different permeability, namely zone of intact rock strata, zone of broken rock strata, zone of fully developed rock fractures and zone of collapsed goaf.

The four distinct zones and their associated gas permeability are detailed in Fig. 14.

The permeability, k, required by FLAC is the mobility coefficient (coefficient of the pore pressure term in Darcy's Law). The relation between hydraulic conductivity, k_h (m/s), commonly used when Darcy's Law is expressed in terms of head, and permeability, k (m^2/Pa s), is:

$$k = \frac{k_h}{g\rho_w}, \tag{9}$$

where g is gravity (m/s^2) and ρ_w is fluid mass density (kg/m^3).

The property of "intrinsic permeability" k_i (m^2) is related to k and k_h as follows:

$$k_i = \mu k,$$

where k_i is the intrinsic permeability (m^2), μ the viscosity (N s/m^2), k the mobility coefficient.

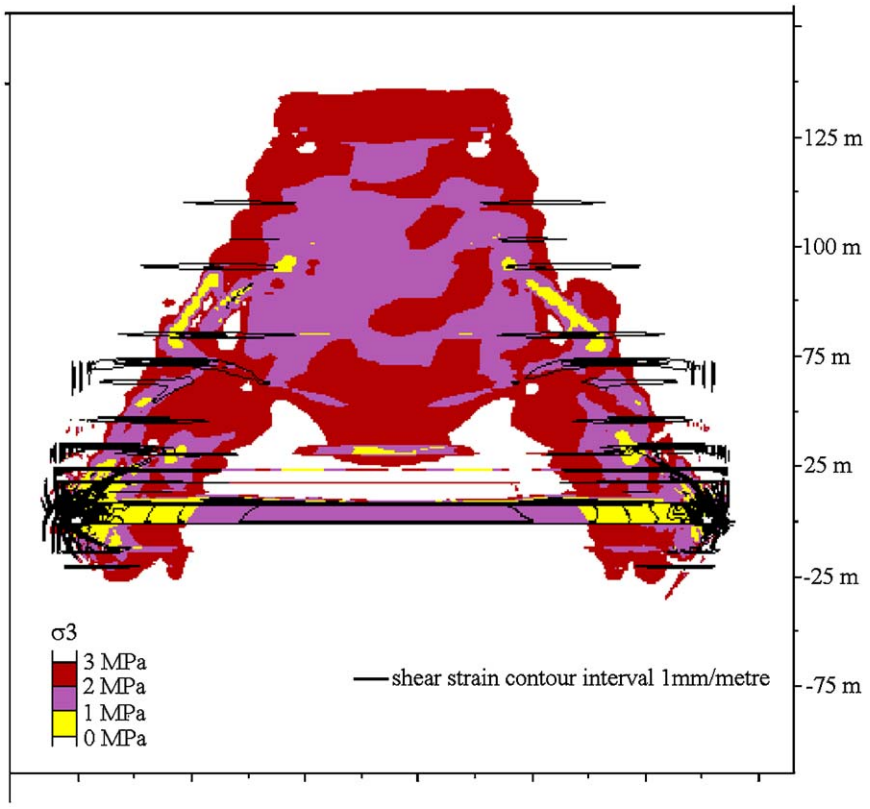

Fig. 12. Model 3: confining stress and shear strain developed around the panel.

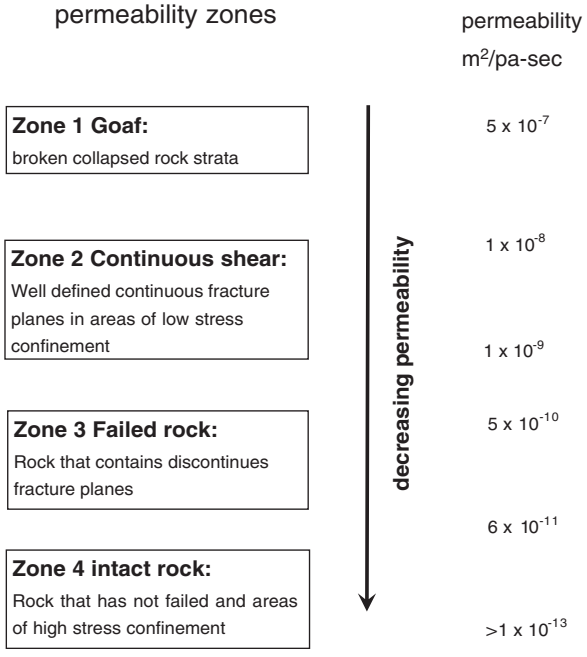

Fig. 13. Zones of gas permeability.

6.1.1. Permeability of intact coal measure rock strata

In the laboratory test work described in Section 4 the intrinsic permeability calculated for the intact samples was below the detection limit of the flow manometers, which gives a value for the intrinsic permeability of the intact rock of less than 1×10^{-19} m^2. This value was adopted for all regions in the model where no yield had occurred. The mobility coefficient was then calculated using Eq. (9) with a gas viscosity of 1.75×10^{-5} N s/m^2.

6.1.2. Permeability of the goaf

Laboratory testing of broken coal measure rocks in a permeameter under different degrees of compaction has been undertaken by Jozefowicz [28]. He tested eight samples consisting of four sandstones, three shales and one gritstone. For the purpose of determining the variation in strata permeability around the panel, a general relationship between state of compaction and permeability was developed using this data by averaging the data and fitting a third degree polynomial curve.

The intrinsic permeability of the goaf was related to the volumetric strain within the goaf using the following relationship:

$$k_{i,goaf} = -4 \times 10^{-16}\,\varepsilon_{vol}^3 - 6 \times 10^{-15}\,\varepsilon_{vol}^2 - 7 \times 10^{-14}\,\varepsilon_{vol} + 1 \times 10^{-11}, \quad (10)$$

where $k_{i,goaf}$ is intrinsic permeability of the goaf (m^2) and ε_{vol} is volumetric strain in the goaf.

The mobility coefficient required in the FLAC modelling was then calculated using Eq. (9) with a gas viscosity of 1.75×10^{-5} N s/m^2.

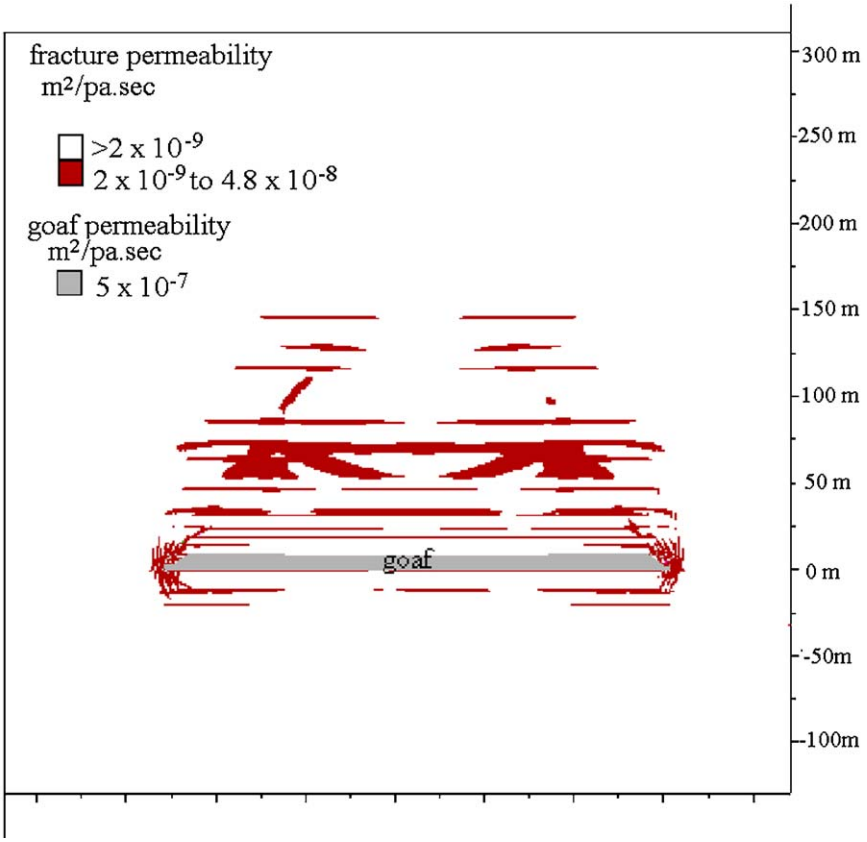

Fig. 14. Goaf permeability, K, from 1×10^{-7} to $5 \times 10^{-7}\,m^2/Pa\,s$; fracture permeability, K, from 2×10^{-9} to $4.8 \times 10^{-8}\,m^2/Pa\,s$.

6.1.3. Permeability of the fracture planes

The permeability of the fracture zones was determined using Eq. (8). From consideration of the permeability testing described in Section 4, an m value of -0.8616 and k_1 permeability of $2.613 \times 10^{-13}\,m^2$ was used within the equation. Again the mobility coefficient, k, was calculated using Eq. (9) with a gas viscosity of $1.75 \times 10^{-5}\,N\,s/m^2$. This viscosity was assumed for both air and the methane gas within the rock strata.

6.1.4. Permeability of yielded rock

This is defined in the models as the regions where the rock has undergone yield but without a fully developed shear plane defined by a total shear strain of 10 mm/m. It was considered that the permeability in these regions would have an upper bound represented by the permeability of a fracture plane. To estimate the permeability of the yielded strata, the stress-dependent permeability for fractured rock (Eq. (8)) was reduced by a factor determined by dividing the shear strain by a shear strain value of 10 mm/m.

6.1.5. Model of rock strata permeability

The functions that predicted the stress-dependent permeability were developed for each of these four regions and coded into the FLAC^{2D} model to predict the distribution of permeability around the panel. The predicted permeabilities for the goaf and rock strata for Model 2 are shown in Fig. 14.

6.2. Methane gas sources

All the coal seams within the model were represented as potential sources of methane gas. The aim of the numerical flow modelling was to predict gas flow paths that would arise from the presence of methane gas within the Parkgate and adjacent coal seams. To simulate the presence of methane gas under pressure with the coal seams, the fluid pressure was fixed at $1 \times 10^6\ N/m^2$ within all the seams. This value was determined from consideration of actual methane pressure measurements obtained for deep coal seams. Direct measurements have been made of seam gas pressures in various countries. For example, pressures of 0.8–1.13 MPa have been recorded in four seams at depths between 820 and 1220 m in China [27]. A pressure of 1.6 MPa has been reported in a seam in the Donbas coalfield at a depth of 644 m, whilst a gas pressure in the range 1.03–1.55 MPa has been reported for a seam in Poland at a depth of 665 m [27].

6.3. Initial conditions

The density of gas present in the rock strata was set at a constant value of 1.225 kg/m^3, which is equivalent to the density of air at sea level. The gas pressure within the rock strata was initialised at 1.01325×10^5 N/m^2 representing atmospheric pressure at sea level. As previously stated the coal seams were considered as potential methane sources and the gas pressure was fixed at a pressure of 1 MPa within the seams.

All UK deep coal mines traditionally employ an exhaust main fan ventilation system whereby the pressure within the entire mine roadway network underground is maintained at pressures below the surface atmospheric pressure. This ventilation regime ensures that whilst the main fan is running a positive pressure gradient exists between the strata and collapsed waste areas, and the mine roadways. Thus, any gas within the strata or waste is under a suction pressure. Should the power to the main fan fail, the mine roadways repressurise and push the potential gas emission back into the relaxed waste areas. During normal operating conditions any methane gas entering the ventilation air from the strata or waste is diluted and removed by the ventilation system. To simulate the pressure differential, the gas pressure on the sides of the roadway was kept fixed at 0.95×10^5 N/m^2, i.e. 0.06325×10^5 N/m^2 below the air pressure in the surrounding rock strata. This lower pressure was also initialised at the start within the goaf but was allowed to vary as gas flow into the goaf occurred.

The gas saturation was assumed to be 1, i.e. fully saturated with respect to gas in the rock strata. The saturation in the edges of the goaf and roadway roof and sides was fixed at zero, i.e. acting as a fluid sink. The porosity was set at 50% for all the rock strata.

In a perfect gas the bulk modulus is equal to the gas pressure. Thus the bulk modulus of the gas in the Deep Soft seam was set at 1 MN/m^2. A lower bulk modulus of 0.1 MN/m^2 was set for the gas outside the seam to account for the lower gas pressures in these regions. However, the bulk modulus of the gas is not critical for determining steady-state conditions as it only influences the prediction in the initial transient flow stage, but has no effect on the flow characteristics once steady-state flow occurs.

6.4. Results of the gas flow modelling

Gas flow modelling was undertaken using the FLAC finite difference time stepping method for solving the Darcian flow problem. The model was run until a steady state flow condition was obtained. Using a Pentium P4, 3.2 GHz computer processor, this took approximately 1 week. Steady-state flow was identified by monitoring pore pressures within the rock strata. The flow pattern around the end of the panel is shown in Fig. 16.

From the figure it can be seen that the major source of the gas is the Deep Hard seam with potentially some flow occurring from the coal seam situated approximately 20 m beneath the floor of the roadway.

Fig. 15 shows a more detailed view of the gas velocity vectors around the tailgate. From the figure it can be seen that the dominant flow paths into the roadway are from the goaf, and from the Deep Hard seam via the roof strata. The modelling shows that gas from the Deep Hard seam flows through the highly fractured roof strata directly into the gate road and also into the roadway via the goaf. (See Fig. 16).

The flow modelling predicted that major source of the gas flowing into the gate roadways was the Deep Hard seam, which lay at a distance of 19 m above the Parkgate seam. Although other coal seams may act as potential gas sources the lack of connectivity of gas flow paths from these seams into the workings prevents the gas flow. An implication of this observation is that coal seams above longwall workings can be disturbed by mining but are unable to release their gas into the mine if the intermediate strata layers are not fractured. Therefore if the gas drainage boreholes are extended to these coal seams, the drainage boreholes may be venting substantially more gas than would have been released into the mine workings by the disturbance created by the mining. However, in practice, it would probably be wise for the mine operator to extend the boreholes into higher seams to reduce the likelihood of emissions occurring into the mine workings caused by variations in the geological conditions.

7. Discussion and conclusions

The FLAC^{2D} and FLAC^{3D} geomechanical and gas flow modelling has provided valuable information to the ventilation engineers responsible for gas drainage for panel 43, Thoresby Colliery.

An analysis of the results predicted by the models concluded that the most likely sources of the methane gas would be from the Deep Hard seam present at approximately 20 m above the roadway. It was further concluded that the most likely flow paths would be through the highly fractured roof stratum directly into the roadway or via the roof stratum and goaf. The results produced by the models also indicated that there was potential for gas flow from a coal seam lying approximately 20 m beneath the roadway. The models also predicted that, although there may be potential gas sources above 20 m over the panel, the confining stresses within the rock strata would reduce the permeability of the strata and gas flow from these sources into the roadway would not occur.

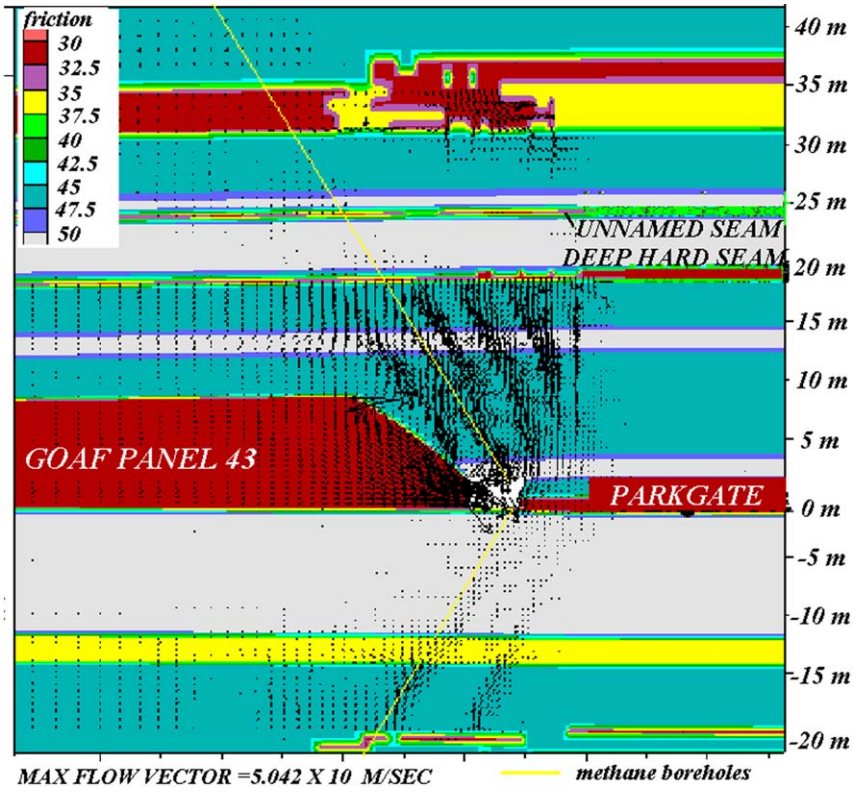

Fig. 15. Fracture permeability, K, from 2×10^{-9} to 4.8×10^{-8} m^2/Pa s.

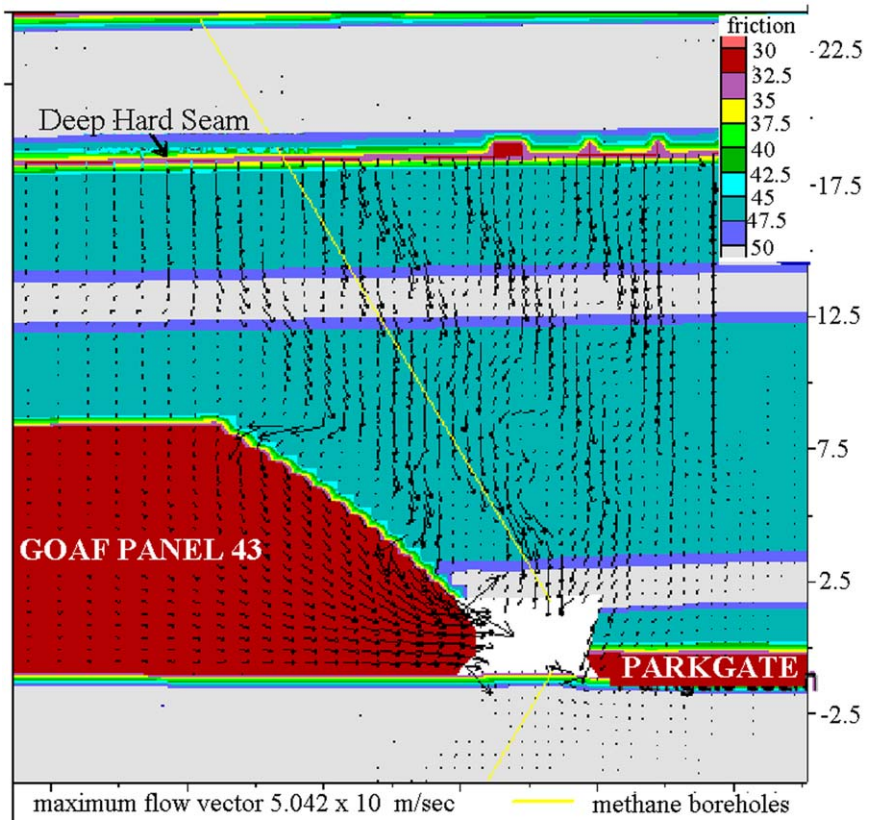

Fig. 16. Flow pattern around the tailgate showing gas velocity vectors.

Of the three stages of goaf compaction modelled namely 10 m, 65 m and greater than 120 m behind the face line, the volume flow rate of gas into the mine workings was greatest at 65 m. This was due to the development of shear planes around the panel and the lower stress conditions present within the immediate roof. With further goaf compaction and distance behind the face line, the reactance of the goaf tended to increase the confining stress within the immediate roof, thus reducing strata permeability.

Around the face line the high stress confinement, and the fact that fracture propagation within the roof strata had not fully developed, precluded gas flow in the rock strata directly overlying the face. This was also observed at Thoresby, where the gas flow in the drainage boreholes only becomes active at distances of approximately 45 m behind the face.

This paper has outlined a methodology of predicting gas flow into longwall mine workings by computer simulation. The simulations require a large amount of input data, especially with respect to the geomechanical conditions, and a large amount of time to construct. For a practical application of the modeling, the authors envisage that a calibrated generic geomechanical model for a specific mine site may be used as a basis for predicting specific gas flow problems on a panel-by-panel basis within that particular mine. It is considered that the generic model may be used for each specific panel but with modifications made on a panel-by-panel basis to allow for variations in panel width, panel orientation, local geological changes and changes in the in-situ stress conditions, etc.

Appendix A. Kirton Borehole

The basic lithological units are presented in Table 6.

Table 6

Strata unit	To base	In metres	Depth relative to base of parkgate
Siltstone + sandstone	1235	376.4	440.7
Seatearth	1238	376.7	440.4
Mudstone	1252	381.6	435.6
Coal + seatearth	1264	385.3	431.9
Siltstone + sandstone	1269	335.8	430.4
Mudstone	1304	397.5	419.7
Coal + seatearth	1309	399.0	418.2
Mudstone + siltstone	1353	412.4	404.8
Seatearth + coal	1374	418.6	398.4
Seatearth	1378	420.0	397.2
Mudstone + siltstone	1395	425.2	392.0
Mudstone	1438	438.3	378.9

Table 6 (*continued*)

Strata unit	To base	In metres	Depth relative to base of parkgate
Seatearth	1445	440.4	376.7
Sandstone	1450	442.0	375.2
Mudstone	1458	444.4	372.8
Fissile mudstone	1459	444.7	372.5
Mudstone	1460	445.0	372.2
Seatearth	1462	445.6	371.6
Mudstone	1465	446.5	370.8
Seatearth	1470	448.1	369.1
Siltstone + sandstone	1475	449.6	367.6
Mudstone	1478	450.5	366.7
Seatearth	1485	452.6	364.5
Siltstone + sandstone	1489	453.9	363.3
Mudstone	1503	458.1	359.1
Sandstone	1523	464.2	353.0
Siltstone + sandstone	1526	465.1	352.0
Mudstone	1537	468.5	348.7
Seatearth	1539	469.1	348.1
Mudstone	1549	472.1	345.0
Coal + seatearth	1554	473.7	343.5
Coal	1555	474.0	343.2
Seatearth	1557	474.6	342.6
Siltstone + sandstone	1565	477.0	340.2
Mudstone	1568	477.9	339.2
Coal + shale	1569	478.2	338.9
Mudstone + siltstone	1585	483.1	334.1
Coal + seatearth	1593	485.6	331.6
Sandstone	1600	487.7	329.5
Coal	1601	488.0	329.2
Seatearth	1603	488.6	328.6
Mudstone	1620	493.8	323.4
Seatearth	1622	494.4	322.8
Mudstone	1628	496.2	321.0
Seatearth	1631	497.1	320.0
Mudstone	1646	501.7	315.5
Seatearth	1649	502.6	314.6
Mudstone	1676	510.9	306.3
Seatearth	1679	511.8	305.4
Mudstone	1683	513.0	304.2
Siltstone + sandstone	1690	515.1	302.1
Mudstone	1699	517.9	299.3
Seatearth	1703	519.1	298.1
Mudstone	1707	520.3	296.9
Seatearth	1711	521.5	295.7
Mudstone	1732	527.9	289.3
Seatearth	1738	529.7	287.4
Mudstone	1757	535.5	281.6
Coal	1758	535.8	281.3
Seatearth	1762	537.1	280.1
Mudstone	1771	539.8	277.4
Coal	1773	540.4	276.8
Seatearth	1778	541.9	275.2
Mudstone + siltstone	1814	552.9	264.3
Mudstone dark grey	1822	555.4	261.8
Sandstone + mudstone	1832	558.4	258.8
Mudstone dark grey	1835	559.3	257.9
Coal	1838	560.2	256.9
Seatearth	1843	561.8	255.4
Siltstone + mudstone	1855	565.4	251.8
Coal (ABDY)	1860	566.9	250.2
Seatearth	1864	568.2	249.0

Table 6 (*continued*)

Strata unit	To base	In metres	Depth relative to base of parkgate
Mudstone + siltstone	1878	572.4	244.8
Seatearth + coal	1881	573.3	243.8
Sandstone, siltstone, mudstone	1885	574.6	245.6
Mudstone	1897	578.2	239.0
Coal	1899	578.8	238.4
Mudstone	1910	582.2	235.0
Shaley mudstone	1914	583.4	233.8
Mudstone	1921	585.5	231.7
Coal	1924	586.4	230.7
Mudstone + siltstone	1940	591.3	225.9
Coal	1941	591.6	225.6
Seatearth	1947	593.5	223.7
Mudstone + siltstone	2023	616.6	200.6
Kent's thick coal	2029	618.4	198.7
Seatearth	2031	619.1	198.1
Mudstone	2042	622.4	194.8
Seatearth + mudstone	2049	624.5	192.6
Mudstone	2072	631.6	185.6
Fissile mudstone	2077	633.1	184.1
Coal	2078	633.4	183.8
Seatearth	2082	634.6	182.6
Mudstone + siltstone	2090	637.0	180.1
Mudstone	2106	641.9	175.3
Cannel coal	2107	642.2	175.0
Mudstone	2127	648.3	168.9
Coal (Top hard)	2132	649.8	167.3
Seatearth	2133	650.1	167.0
Mudstone	2137	651.4	165.8
Mudstone + siltstone + sandstone	2184	665.7	151.5
Coal (Dunsil)	2192	668.1	149.0
Seatearth	2195	669.0	148.1
Mudstone + sandstone	2235	681.2	135.9
Mudstone	2247	684.9	132.3
Seatearth + coal	2251	686.1	131.1
Mudstone	2257	687.9	129.2
Seatearth + coal	2260	688.9	128.3
Siltstone + mudstone	2285	696.5	120.7
Seatearth + coal	2286	696.8	120.4
Mudstone	2291	698.3	118.9
Mudstone + coal + seatearth	2299	700.7	116.4
Mudstone + siltstone	2318	706.5	110.6
Fissile mudstone	2320	707.1	110.0
Mudstone	2353	717.2	100.0
Coal (Lidgett)	2354	717.5	99.7
Mudstone	2396	730.3	86.9
Seatearth + coal	2404	732.7	84.4
Mudstone + siltstone	2440	743.7	73.5
Mudstone dark grey	2461	750.1	67.1
Fissile mudstone	2462	750.4	66.8
Seatearth + coal	2468	752.3	64.9
Mudstone	2481	756.2	61.0
Seatearth	2482	756.5	60.7
Mudstone	2508	764.4	52.7
Mudstone + coal + seatearth	2510	765.1	52.1
Mudstone	2524	769.3	47.9
Seatearth + coal	2528	770.5	46.6
Mudstone + siltstone	2558	779.7	37.5
Coal (Deep soft)	2565	781.8	35.4
Seatearth + coal	2578	785.8	31.4
Siltstone + sandstone	2595	791.0	26.2

Table 6 (*continued*)

Strata unit	To base	In metres	Depth relative to base of parkgate
Mudstone	2600	792.5	24.7
Coal + seatearth	2601	792.8	24.4
Mudstone	2617	797.7	19.5
Cannel coal (Deep hard)	2618	798.0	19.2
Seatearth	2620	798.6	18.6
Mudstone + siltstone	2634	802.9	14.3
Mudstone	2640	804.7	12.5
Sandstone + siltstone	2669	813.5	3.7
Mudstone	2675	815.3	1.8
Coal (Parkgate)	2681	817.2	0.0
Seatearth	2687	819.0	−1.8
Mudstone	2721	829.4	−12.2
Fissile mudstone	2723	830.0	−12.8
Mudstone + seatearth	2729	831.8	−14.6
Seatearth	2730	832.1	−14.9
Mudstone + sandstone	2745	836.7	−19.5
Coal (Low Tupton)	2746	837.0	−19.8
Seatearth	2752	838.8	−21.6
Coal (Three quarters)	2754	839.4	−22.3
Seatearth	2756	840.0	−22.9
Sandstone	2763	842.2	−25.0
Mudstone	2807	855.6	−38.4
Coal (Blackshale)	2813	857.4	−40.2
Mudstone + seatearth	2831	862.9	−45.7
Sandstone + siltstone + mudstone	2851	869.0	−51.8
Sandstone	2895	882.4	−65.2
Mudstone	2904	885.1	−68.0

References

[1] Hargreaves DM, Moloney KW, Pearce W, Lowndes IS. Validation of computational models of auxiliary ventilation systems with experimental data. Proceedings of the eigth US Mine Ventilation Systems, Rollo, SME.

[2] Creedy DP, Saghafi A, Lama R. Gas control in underground coal mining, IEA Coal Research, 1997, ISBN: 92-9029-280-6.

[3] Whittles DN. Application of rock mass classification principles to coal mine design. PhD thesis, University of Nottingham, 1999.

[4] Itasca Consulting Group Inc. FLAC Version 4 Users manual. Itasca, Consulting Group, Inc., Minneapolis, 2000.

[5] Mohammad N. An investigation into the effect of stress on the permeability of rock taken from carboniferous strata. PhD thesis, University of Nottingham, 1971.

[6] Mordecai M. An investigation into the effect of stress on the permeability of rock taken from carboniferous strata. PhD thesis, University of Nottingham, 1971.

[7] Neate CJ. Effects of mining subsidence on the permeability of coal measure rocks. PhD thesis, University of Nottingham, 1980.

[8] Durucan S. An investigation into the stress permeability relationship of coals and flow patterns around working longwall faces. PhD thesis, University of Nottingham, 1981.

[9] Keen TF. The simulation of methane flow in carboniferous strata. PhD thesis, University of Nottingham, 1977.

[10] O'Shaughnessy SM. The computer simulation of methane flow through strata adjacent to a working longwall face. PhD thesis, University of Nottingham, 1980.

[11] Watt AW. The movement of gases in longwall coalface waste liable to spontaneous combustion. PhD thesis, University of Nottingham, 1987.
[12] Ediz IG. An application of numerical methods to the prediction of strata methane flow in mining. PhD thesis, University of Nottingham, 1991.
[13] Brandt J. Control of gas emissions at high performance longwalls in the German hard coal mining industry. Proceedings of the seventh International Mine Ventilation Congress, Krakow, Poland, p. 119–25 [Chapter 19].
[14] Kunz E. Gas emission problems in straining the workings and control measures. Proceedings of the seventh International Mine Ventilation Congress, Krakow, Poland, p. 105–8 [Chapter 17].
[15] Ren TX, Edwards JS. Application of CFD techniques to methane prediction and control in coal mines. Proceedings of the 27th International Symposium on Computer Applications in the Minerals Industry, 19–23 April London, UK: The I.M.M; 1998. p. 733–44.
[16] Moloney KW, Hargreaves DM, Lowndes IS. Assessment concerning the accuracy of computational fluid dynamics (CFD) simulations in underground auxiliary ventilated headings. Proceedings of APCOM XXVI London. London: IMM; 1998. p. 721–32.
[17] Hargreaves DM, Moloney KW, Lowndes IS. Preliminary computational fluid dynamics (CFD) simulations of methane dispersion in a heading. Proceedings of the second International Symposium on Mine Environmental Engineering, Brunel, UK, 1998.
[18] ITASCA. FLAC^{3D}, Version 2.1. Minneapolis, Minnesota, USA: Itasca Consulting Group Inc.; 2002.
[19] DTI. A review of the remaining reserves at deep mines. Prepared for the Department of Trade and Industry by IMCL Ltd., December 2002.
[20] Bieniawski ZT. Rock mass classification in rock engineering. Proceedings of the Symposium on Exploration for Rock Engineering, Johannesburg, vol. 1. Rotterdam: AA Balkema; 1976. p. 97–106.
[21] Barton N, Lein R, Lunde J. Analysis of rock mass quality and support practice in tunneling, and a guide for estimating support requirements, Internal report, Norges Geotekniste Institutt; 1974. p. 1–74.
[22] Hoek E, Brown ET. Practical estimates of rock mass strength. Int J Rock Mech Min Sci Geomech Abstr 1997;34(8):1165–86.
[23] Mitri HS, Edrissi R, Henning J. Finite element modelling of cable bolted stopes in hard rock underground mines. Presented at the SME Annual Meeting, Albuquerque, NM, February 1994, Paper no. 94–116 (Case 33).
[24] Truman R. A finite element analysis for the establishment of stress development in coal mined caved waste. Mining Sci Technol 1990(10):247–52.
[25] Thin IGT, Pine RJ, Trueman R. Numerical modelling as an aid to the determination of the stress distribution in the goaf due to longwall coal mining. Int J Rock Mech Min Sci Geomech Abstr 1993;30:1403–9.
[26] Yavuz H. An estimation method for cover pressure re-establishment distance and pressure distribution in the goaf of longwall coal mines. Int J Rock Mech Min Sci Geomech Abstr 2004;41:193–205.
[27] IEA Coal Research. Gas control in underground mining. April 1997; Principal authors: Creedy DP, Saghafi A, Lama R.
[28] Jozefowicz RR. The post failure stress permeability behaviour of coal measure rocks. PhD thesis, University of Nottingham, 1997.
[29] Anderton R, Bridges PH, Leeder MR, Sellwood BW. A dynamic stratigraphy of the British isles. London: George Allen and Unwin; 1983.
[30] Bigby DN, Cassie JW, Ledger AR. Absolute stress and stress change measurements in British coal measures. In: Hudson JA, editor. ISRM Symposium: Eurock '92. Thomas Telford; 1992. p. 390–5.
[31] Anon. Assessment of retreat options and maingate support requirements for Rossington with initial application to B100's unit. Interim Report-Stage 1, Rock Mech Technol, May 1997.
[32] Peng SS, Chiang HS. Longwall mining. New York: Wiley; 1984.
[33] Wilson AH. The stability of underground workings in the soft rocks of the coal measures. Int J Mining Eng 1983;1:91–187.
[34] Reddish DJ, Stace LR, Whittles DN. The utilisation of numerical modelling to predict water and gas flows around longwall panels; two case studies from the UK Coal Mining Industry. Proceedings of the 22nd International Conference on Ground Control in Mining, Morgantown, USA, 2003.
[35] Denby B. Shear strain assessment in mine slope design. PhD thesis, University of Nottingham, 1983.